Journal of Materials Chemistry C

Materials for optical and electronic devices

www.rsc.org/MaterialsC

Volume 1 | Number 34 | 14 September 2013 | Pages 5171–5430

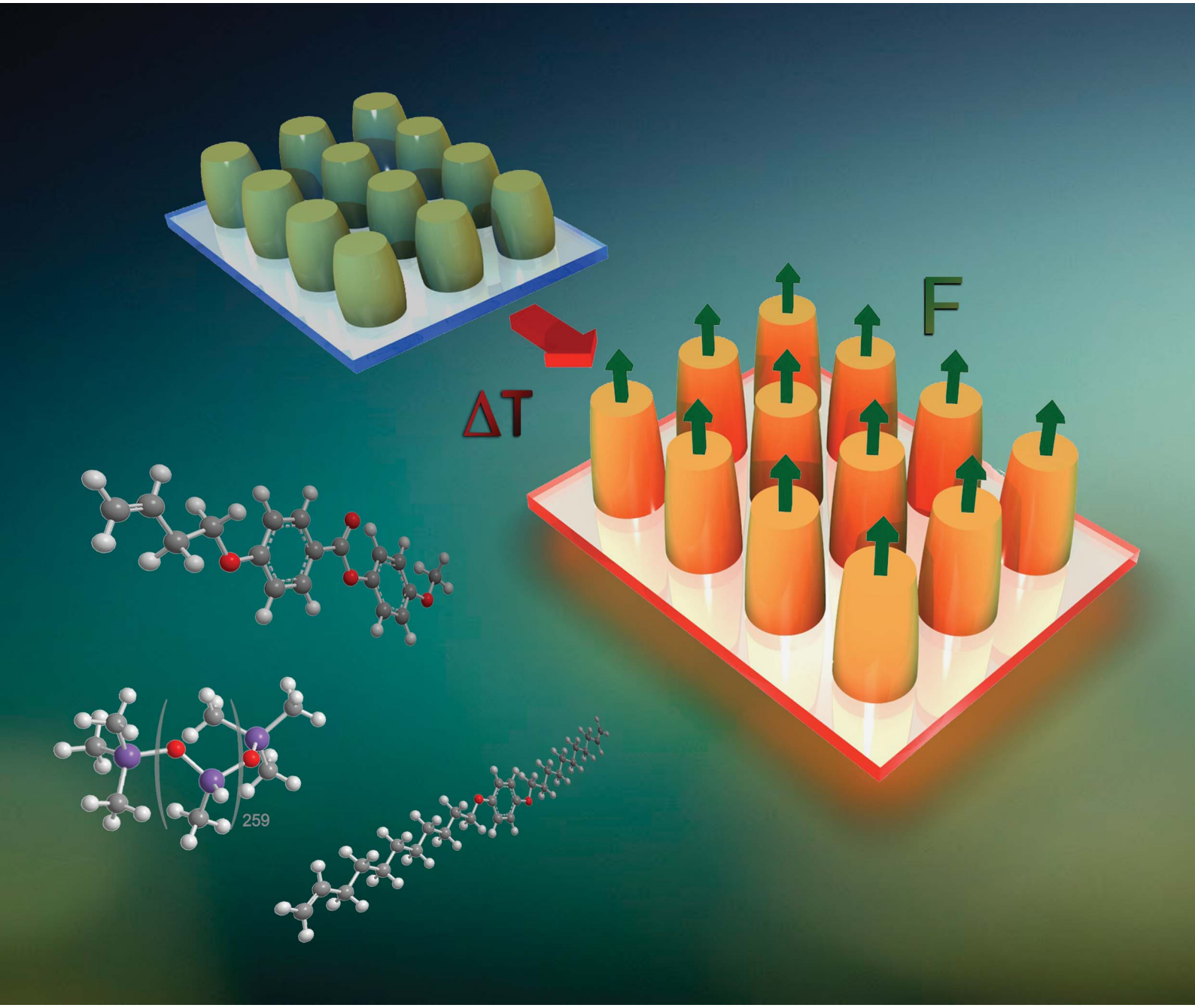

ISSN 2050-7526

RSC Publishing

PAPER

Jaume Esteve, Antoni Sánchez-Ferrer *et al.*

Liquid-crystalline elastomer micropillar array for haptic actuation

2050-7526(2013)1:34;1-C

Journal of Materials Chemistry C

RSC Publishing

PAPER

Liquid-crystalline elastomer micropillar array for haptic actuation†

Cite this: *J. Mater. Chem. C*, 2013, **1**, 5183

Núria Torras,[ab] Kirill E. Zinoviev,‡[a] Jaume Esteve*[a] and Antoni Sánchez-Ferrer*[c]

Received 10th June 2013
Accepted 12th July 2013

DOI: 10.1039/c3tc31109k

www.rsc.org/MaterialsC

A new liquid-crystalline elastomer-based micropillar array with pushing properties is obtained by the two-step crosslinking process, where the micropillars are oriented by uniaxial compression before the final curing. This orientation process allows the formation of a two-dimensional prolate polydomain conformation of the polymer backbone and the mesogens, and opens huge opportunities for the use of liquid-crystalline elastomers in microsystems and haptic applications.

Introduction

The combination of the liquid crystal anisotropy and the entropy elasticity of polymer networks results in materials with unique physical properties: liquid-crystalline elastomers (LCEs).[1] The most relevant property of such materials is the anisotropically macroscopic change in shape when a mono-domain of LCE becomes disordered by means of any external stimulus (*e.g.* light,[2,3] magnetic[4,5] or electric fields[6,7]). A huge deformation appears due to the shrinkage of the polymer backbone with prolate conformation along the director.[8,9] Both the change in length and the mechanical properties of LCEs[10,11] are strongly affected by the type of mesogens, the crosslinking density, and the attachment of the liquid-crystalline molecules to the polymer backbone.[12,13]

Microactuators can be designed based on LCEs, opening new possibilities for microengineering. The first lab-scale LCE materials for microdevices were synthesized by radical polymerization of acrylate-based mesogens, by aligning them under magnetic fields, and resulting in LCE actuators as micropillars,[14] or by using microfluidics for obtaining spherical monodisperse particles.[15] In both cases, the nematic-to-isotropic temperature was rather high (120 to 140 °C) – with a high glass transition or even crystallization temperature around 100 °C – and deformations upon heating the material were in the range of 25 to 35%. Previous works on using LCEs for the development of the microsystem technology have been performed by using low glass transition temperature networks based on siloxane chemistry.[16,17]

Due to the great actuating and sensing properties of such materials, a new scenario for the use of LCEs has appeared for haptic technology where interfaces can interact with the user *via* the sense of touch. Carbon nanotubes (CNTs) are introduced into the LCE matrix which had been punched in order to create a 3D structure out of the LCE film.[18] Thus, light was absorbed because of the presence of the CNTs, and heat was released into the nanocomposite material, with the corresponding isotropization and shrinkage of the sample.[19]

In this work, we present a successful nematic side-chain liquid-crystalline elastomer micropillar array which expands in the direction of the applied orientation when the isotropic temperature is reached. This pushing behavior of the micropillars is related to the changes from the two-dimensional prolate polydomain conformation (nematic state) to the spherical conformation (isotropic state) of the polymer backbone.

Experimental

Synthesis of the mesogen and crosslinker

The rod-like side-chain mesogen (SCM) and the isotropic side-chain crosslinker (SCC) were synthesized as described in previous papers.[20–23]

Synthesis of the nematic side-chain liquid-crystalline elastomer micropillar array

The oriented nematic LCE micropillar array was prepared using a new orientational process, where both the mesogens and the polymer backbones show a planar orientation. After the non-complete hydrosilylation reaction,[24,25] the sample was partially deswollen and removed from the reactor/mold and aligned by applying uniaxial compression perpendicular to the cylindrical axis. The curing process allowed the completion of the

[a]*Instituto de Microelectrónica de Barcelona, IMB-CNM (CSIC), Campus UAB, Bellaterra, E-08193 Barcelona, Spain. E-mail: jaume.esteve@imb-cnm.csic.es*

[b]*Departament de Microelectrònica i Sistemes Electrònics, Universitat Autònoma de Barcelona, Campus UAB, Bellaterra, E-08193 Barcelona, Spain*

[c]*ETH Zurich, Department of Health Sciences & Technology, Institute of Food, Nutrition & Health, Food & Soft Materials Science Group, Schmelzbergstrasse 9, CH-8092 Zurich, Switzerland. E-mail: antoni.sanchez@hest.ethz.ch*

† Electronic supplementary information (ESI) available: Thermoelastic and mechanical setups, and swelling experiments. See DOI: 10.1039/c3tc31109k

‡ Present address: Medlumics SL, Ronda de Poniente 16 1E, 28760 Tres Cantos, Madrid, Spain.

hydrosilylation reaction, while maintaining the compression of the sample – second step of the crosslinking reaction in the nematic phase during the orientation of the samples. The nematic LCE was synthesized using 20 mol% of crosslinking double bonds or 11.1 mol% of a crosslinker (Scheme 1). For this crosslinking composition, the sample has 16 side-chain repeating units between two crosslinkers.

In a 5 mL flask, 477 mg (1.60 mmol) of the side-chain mesogen (SCM) 4-methoxyphenyl 4-(but-3-en-1-yloxy)benzoate, 83 mg (0.20 mmol) of the isotropic side-chain crosslinker (SCC) 1,4-bis(undec-10-en-1-yloxy)benzene, and 120 mg (2.00 mmol SiH) of poly(methylhydrosiloxane) (PMHS, DP = 259) were placed. To this mixture, 2 mL of thiophene-free toluene and 40 μL of 1%-Pt cyclooctadieneplatinum(II) chloride, $Pt(COD)Cl_2$, in dichloromethane were added. The reactive mixture was filled in the holes of the Teflon mold which was heated at 70 °C in an oven for 1 h 45 min. Afterwards, the reactor/mold was cooled and the elastomer micropillar array was removed. In this first step the elastomer is not totally crosslinked. Some pressure was applied by fixing the distance between two Teflon plates in order to align the sample during the deswelling process, and in order to fix this orientation, the crosslinking reaction was completed by leaving the elastomer in the oven under a vacuum at 70 °C for 2 days.

Apparatus and techniques

The phase transformation behavior of the LCE micropillars was investigated by Differential Scanning Calorimetry (DSC) measurements using a Perkin Elmer DSC8500 differential scanning calorimeter equipped with a liquid nitrogen controller Cryofill at heating/cooling rates of dT/dt = 5, 10, and 20 K min^{-1}. The first order transition temperatures were determined by extrapolating the heating/cooling rate to 0 K min^{-1}. The glass transition temperature (T_g) was determined by the half-vitrification temperature ($1/2\Delta C_p$). The nematic-to-isotropic phase transformation temperature (T_{NI}) was determined by temperatures of the maxima of the heat flow. The changes in the heat capacity (ΔC_p) and the latent heat (ΔH_{NI}) were calculated from the thermograms.

Swelling experiments were performed in toluene at 25 °C in order to obtain information about the effective crosslinking density and the anisotropy of the network. The dimensions of the LCE micropillars were determined using a Will Strübin-Wetzlar optical microscope. The volumetric swelling parameter $q = V/V_0 = \alpha_r^2\alpha_z$ is the ratio of the volume of the swollen to dry elastomer. The anisotropy of the swelling q_z is defined as $q_z = \alpha_z/\alpha_r$, where α_z and α_r are the swelling ratios parallel (axial) and perpendicular (radial) to the cylindrical axis, respectively, during the swelling process.

X-ray diffraction experiments were performed using a Philips PW 1730 rotating anode (4 kW) in order to obtain direct information on the WAXS reflections in the nematic phase. Cu K_α radiation (1.5418 Å) filtered by a graphite monochromator and collimated by a 0.8 mm collimator was used. The incident beam was normal to the surface of the film. The scattered X-ray intensity was detected by a Schneider image plate system (700 × 700 pixels, 250 μm resolution). From the WAXS intensities, the

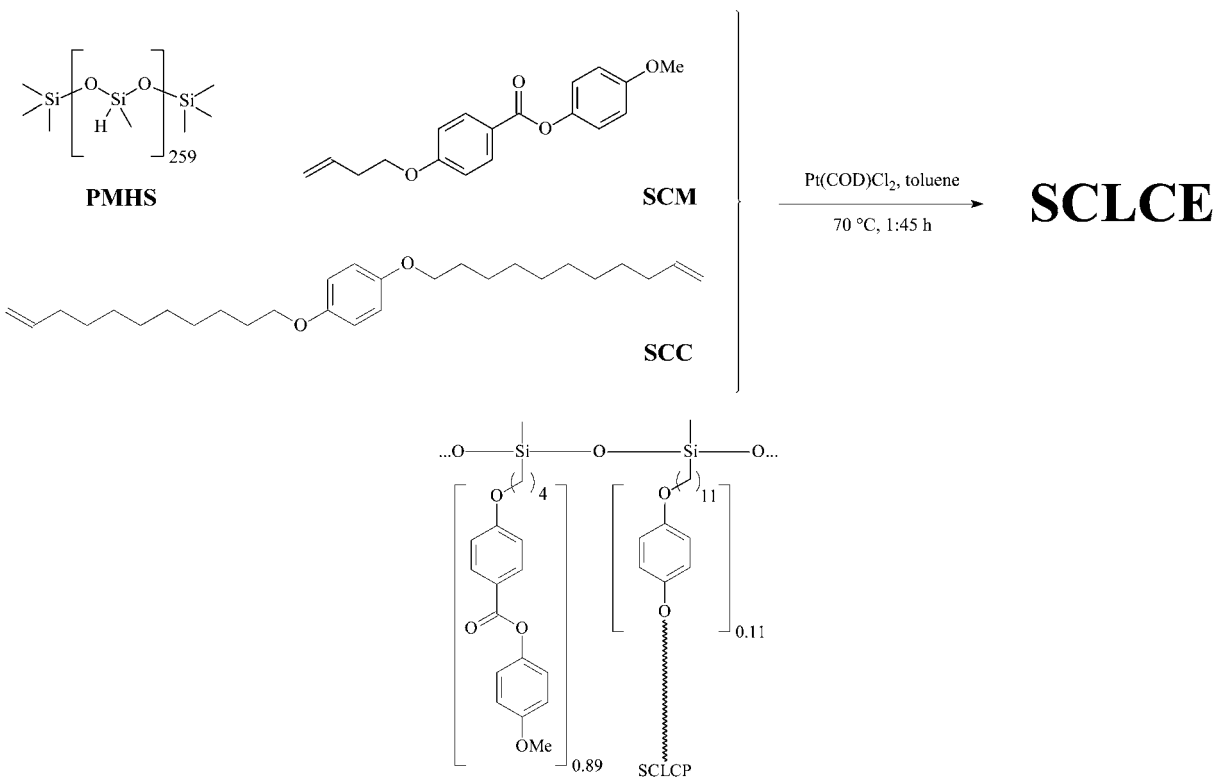

Scheme 1 Synthetic route to the nematic side-chain liquid-crystalline elastomer SCE-10.

mean mesogen-to-mesogen and the mean polymer-to-polymer distances (d_m and d_p), and the mesogen and polymer backbone angle distributions (ϕ) were calculated using a Gaussian distribution, and the order parameter ($S = S_d \cdot S_N$) was determined according to Lovell and Mitchell,[26,27] where S_d is the director order parameter and S_N the order parameter that refers to the local orientational order parameter. For samples having a macroscopically uniform alignment of the director we assume that $S_d \approx 1$.

Optical microscopy experiments were performed using a Nikon Eclipse ME600 polarized light optical microscope, equipped with a Nikon DXM 1200F digital camera.

Thermoelastic experiments were performed with a self-constructed apparatus designed to measure the length and diameter of a LCE micropillar as a function of temperature (Fig. ESI-1†). After cutting and placing one LCE micropillar on a self-constructed micro-hotplate with controlled atmospheric chamber and temperature (ITC 510, Thorlabs), pictures were recorded with a Moticam 2300 3.0 MPixels digital camera mounted on a Leica DM LM upright optical microscope. The change in radius ($\lambda_r = d/d_{ISO}$) and height ($\lambda_z = h/h_{ISO}$) was calculated by evaluation of the optical pictures with the image processing software ImageJ 1.47.

In order to measure the mechanical actuation of the sample, the LCE micropillar array was heated from room temperature to 90 °C using a self-constructed miniaturized hotplate, which consisted of a Peltier (TEC 1.4-6, Thorlabs) placed between two aluminum plates in order to stabilize and homogenize the temperature. Temperature was monitored by a temperature sensor coupled to a power controller (ITC 510, Thorlabs). The force (stress) generated during the expansion of the LCE micropillars when heated was measured using a dynamometer (M5-025, MARK-10) with a resolution $\Delta F = 0.05$ mN, which was in contact with the top surface of one single LCE micropillar. The use of microtranslational stages allows the correct relative positioning between these elements. The dynamometer was coupled to a computer, and all relevant data like temperature, time and measured force were acquired by self-developed data acquisition software. Two complete heating and cooling cycles were recorded and analyzed for each LCE micropillar (Fig. ESI-2†), showing good repeatability in the results from the two cycles.

The Teflon templates for the LCE micropillars were micromechanized in PTFE to avoid any degradation during the evaporation of solvents and at high temperatures. The dimensions of the holes in the Teflon templates were calculated taking into account the volume fraction of non-volatiles which are the constituents of the final LCE micropillar. Some 30 mm side square Pyrex substrates with 0.5 mm thickness were chosen to ensure good heat transfer to the LCE micropillars. All Pyrex substrates were first treated with allyltrichlorosilane (95%, ABCR) in order to guarantee a strong chemical adhesion of the LCE micropillars to the substrate, by depositing few drops of the reactive silane on the Pyrex surface under nitrogen atmosphere. The deformation of the LCE micropillars was induced by applying a homogeneous uniaxial compression along the vertical axis of the LCE micropillars before the final crosslinking process of the material. Thus, from the original height of 3.63 mm after the first crosslinking stage, the micropillars were uniaxially deformed to 3.00 mm ($\lambda = 0.83$) by fixing their height after the second crosslinking process. This uniaxial compression (biaxial deformation) is the key step of the preparation process for the alignment of the sample, and together with the crosslinking density, will define the final expansion ratio of the LCE micropillars. In the nematic state, the LCE micropillars have average dimensions of 3.00 mm in height and 2.46 mm in diameter. After heating the LCE array to the isotropic phase, the average dimensions of the micropillars changed to 3.63 mm in height and 2.10 mm in diameter.

Results and discussion

Liquid-crystalline elastomer micropillar array preparation

The orientated nematic LCE micropillar array was prepared using a new orientational process, where both the mesogens and the polymer backbone show a planar orientation. The mixture of mesogen, crosslinker, polymer backbone, and catalyst in toluene was placed in the reactor/mold gaps (Fig. 1a), and removed after the non-complete hydrosilylation reaction at 70 °C. The sample was partially deswollen and removed from the reactor/mold (Fig. 1b), and aligned by imposing a uniaxial compression (biaxial deformation) in the direction of the cylindrical axis (Fig. 1c). The curing process allowed the completion of the hydrosilylation reaction, while maintaining the compression of the sample (Fig. 1d) – second step of the crosslinking reaction in the isotropic phase at 70 °C during the orientation of the sample.

Using this deformation approach, a two-dimensional prolate polydomain conformation of the polymer backbone together with the mesogens should be expected, which corresponds to a preferred planar orientation (Fig. 2). Thus, when isotropization of the nematic liquid-crystalline elastomer takes place, an expansion along the direction where the uniaxial compression was applied and a contraction in the other two directions perpendicular to the applied deformation direction will be measurable (Fig. 1e). Indeed, this two-dimensional prolate polydomain conformation will lead to a new deformation mechanism for LCEs upon isotropization. Conventional prolate LCEs are uniaxially oriented, and this deformation induces shrinkage along the macroscopic orientational direction upon heating the sample. In contrast, two-dimensional prolate polydomains of LCEs which can be obtained by uniaxial compression (or an equivalent biaxial orientation) induce the opposite effect: expansion along the macroscopic deformation direction. The anisotropic deswelling method has been used for the synthesis of two-dimensional prolate polymer conformations in cholesteric LCEs for tunable mirrorless lasing,[28] but only expansions of 12% in the direction of deswelling were obtained,[29] and this method cannot be applied for the production of cylinder-like objects. Moreover, the actuation principle for the LCE micropillars consists of using an external stimulus to induce an expansion along the cylinder axis (λ_z) and shrinkage in the radial direction (λ_r) as shown in Fig. 1e.

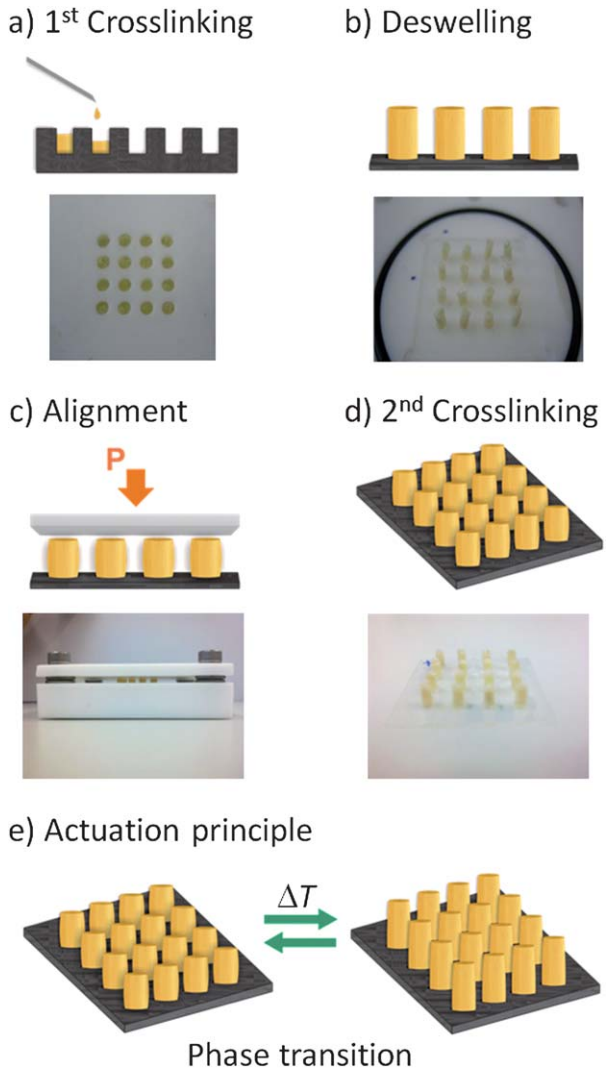

Fig. 1 Schematic diagram showing how the LCE micropillar array was obtained: (a) weakly crosslinked sample obtained by casting the reagents into the Teflon mold, (b) unmolding and deswelling of the LCE micropillar array, (c) alignment of the LCE micropillar array by axial compression, and (d) final shape of the LCE micropillar array after curing the sample. (e) Actuation principle of the micropillar array by means of a phase transition with a macroscopic expansion along the axial direction of the micropillars upon heating.

Liquid-crystalline elastomer micropillar array characterization

The thermal properties of the micropillars were evaluated by DSC experiments, showing a glass transition temperature $T_g = -9$ °C with a change in the heat capacity $\Delta C_p = 0.470$ J K^{-1} g^{-1} characteristic of polysiloxane-based liquid-crystalline elastomers, and a clearing temperature $T_{NI} = 57.2$ °C with a transition enthalpy $\Delta H_{NI} = 1.23$ J g^{-1} common for nematic elastomers (Fig. 3). These temperature values show that the material is suitable for actuation: it has a soft and flexible polymer backbone, with a relatively low actuation temperature. In order to investigate the order in the micropillar in the nematic phase, swelling, X-ray, and polarized optical microscopy experiments were performed at room temperature.

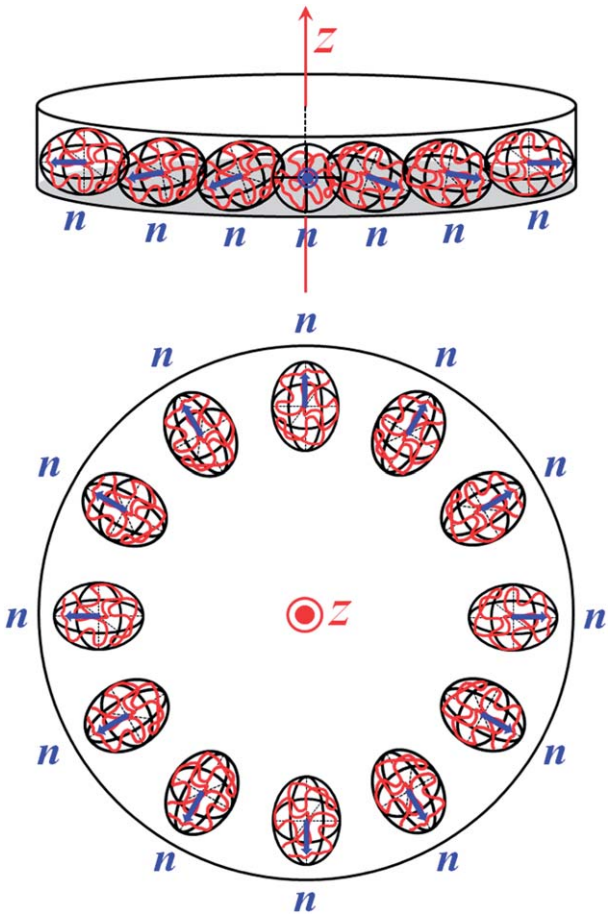

Fig. 2 Nematic two-dimensional prolate polydomain conformation of the planar oriented mesogens and polymer backbone.

Swelling experiments were done using toluene as a solvent at room temperature, and values for the swelling ratios α_r and α_z of 1.56 ± 0.04 and 1.71 ± 0.05 were obtained, respectively. The

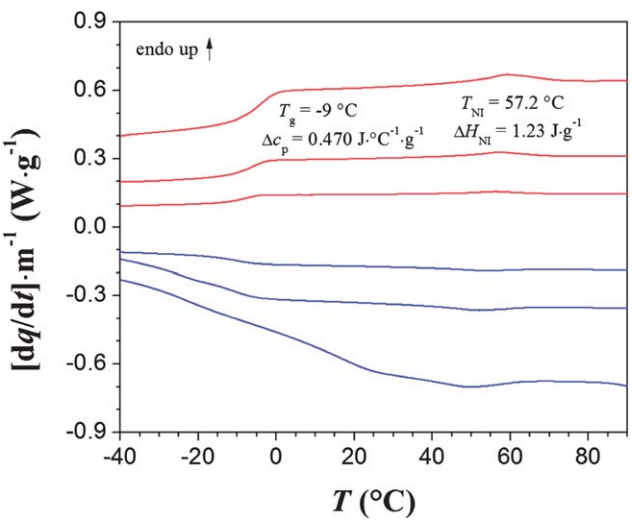

Fig. 3 DSC curves on a nematic liquid-crystalline elastomer micropillar at the heating/cooling rates dT/dt = 20, 10 and 5 K min^{-1}.

higher value for the swelling ratio along the axial cylindrical direction already indicates a more compressed state in this direction with respect to the radial one. Usually, non-oriented samples show swelling anisotropy values equal to the unit, and for this radial prolate polydomain sample the swelling anisotropy value $q_z = \alpha_z/\alpha_r$ of 1.10 ± 0.04 indicates that the sample swells more in the *z*-axis. This anisotropically enhanced swelling capacity manifests as an effect of the applied compression during the alignment of the sample, which leads to an extra expansion when incorporating solvent molecules in the swollen isotropic state. Furthermore, the swelling parameter $q = 4.2 \pm 0.3$ has a value which is close to that for side-chain LCE samples with a crosslinker content of 10 mol%.[2,29] Other samples were prepared and analyzed at different synthetic steps, and the effect on their swelling behavior was evaluated (Fig. ESI-3†). A partially crosslinked non-oriented micropillar swells more than a fully crosslinked micropillar, and the swelling anisotropy values of a fully crosslinked oriented micropillar are higher than those in the non-oriented samples.

X-ray experiments were also performed at room temperature, and the two directions (axial and radial) were analyzed by placing the beam perpendicular to each of them. The analysis of the sample when the X-ray beam was perpendicular to the cylindrical axial direction (*z*-axis) (Fig. 4a) showed a 2D X-ray pattern with two maxima in the meridian (Fig. 4b), which corresponds to a distribution of mesogens in the plane parallel to the circular cross-section of the micropillars. Deeper insight into the orientation of the material was obtained by means of XRD, where the 1D X-ray pattern (Fig. 4c) shows two maxima at distances $d_p = 8.6$ Å ($q_p = 7.35$ nm^{-1}) and $d_m = 4.4$ Å ($q_m = 14.3$ nm^{-1}), which correspond to the polymer and the mesogen distance, respectively. The azimuthal analysis of these two previously indicated distances shows two maxima at 90° and 270° for both distributions (Fig. 4d). Thus, a radial prolate polydomain conformation for both the polymers and the mesogens is present in the oriented micropillars. The calculated order parameters for both distributions were negative, with values of $S_p = -0.35$ and $S_m = -0.33$ in agreement with ordered radial distribution of domains in the cylindrical plane of both the polymer and the nematogen. The measurement performed when the X-ray beam was parallel to the cylindrical axial direction (*z*-axis), as indicated in Fig. 4e, showed a random distribution of the nematic domains, with no maxima in the 2D X-ray pattern (Fig. 4f), and no maxima in the azimuthal distribution of both the mesogen and the polysiloxane polymer backbone (Fig. 4h). The 1D X-ray pattern (Fig. 4g), in contrast, showed features similar to those of the measurement done with the X-ray beam perpendicular to the *z*-axis.

Polarized optical microscopy experiments were performed on a micropillar section perpendicular to the cylindrical axis in order to investigate the nature of the planar orientation of the mesogens as observed previously by X-ray experiments. The results confirmed the two-dimensional prolate polydomain conformation where birefringence was always present in the sample when measuring the sample at different rotating angles (Fig. 5).

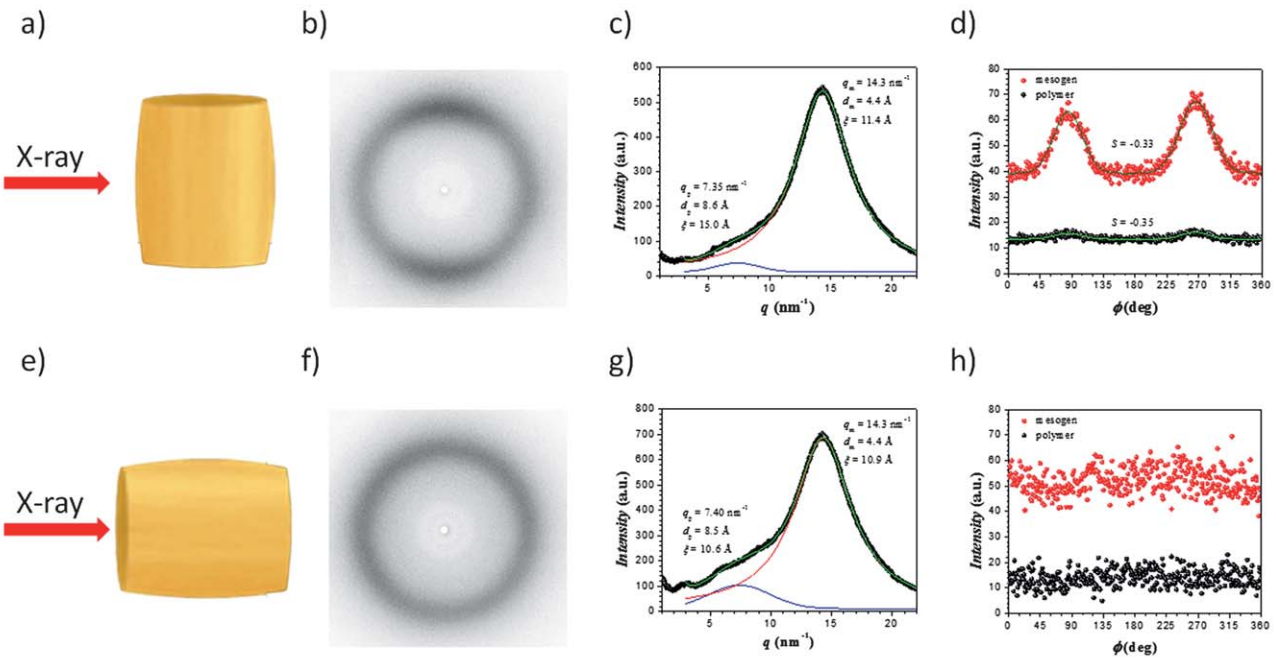

Fig. 4 Confirmation of the nematic planar orientation of the LCE micropillars by XRD experiments: (a) X-ray beam perpendicular to the axial direction of the micropillar, (b) 2D XRD pattern with two maxima in the meridian, (c) 1D XRD radial intensity distribution with two maxima at 8.6 Å and 4.4 Å corresponding to the polymer–polymer distance and the mesogen–mesogen distance, respectively, and (d) azimuthal XRD intensity distribution of the mesogens and the polymer backbone; (e) X-ray beam parallel to the axial direction of the micropillar, (f) 2D XRD pattern with no maxima, (g) 1D XRD radial intensity distribution with two maxima at 8.5 Å and 4.4 Å corresponding to the polymer–polymer distance and the mesogen–mesogen distance, respectively, and (h) azimuthal XRD intensity distribution of the mesogens and the polymer backbone.

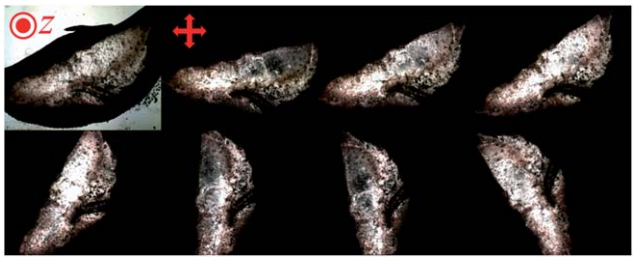

Fig. 5 Optical microscopy images of the cross-section perpendicular to the cylindrical axis of a micropillar with non-polarized light (top-left image) and with polarized light at different rotating angles with respect to the polarizers, showing the presence of microdomains which are distributed radially in the plane.

Thus, the polydomain was structurally proven due to the scattering of the sample and the presence of microdomains distributed radially in the plane of the cylinder.

Liquid-crystalline elastomer micropillar array actuation

The change in the dimensions was optically evaluated on a temperature range from room temperature to the isotropic state in order to investigate the mechanism from the two-dimensional prolate polydomain conformation to the spherical conformation of the polymer chains and mesogens.

In the nematic state, the LCE micropillars have average dimensions of 3.00 mm in height and 2.46 mm in diameter. After heating the LCE array to the isotropic phase, the average dimensions of the micropillars changed to 3.63 mm in height and 2.10 mm in diameter (Fig. 6a and b). These results are summarized in the thermoelastic plot (Fig. 6c), where the change in length in the axial (λ_z) and radial (λ_r) directions is shown as a function of temperature. A clear change in both directions is observed, with values at room temperature of λ_r (22 °C) = 1.17 and λ_z (22 °C) = 0.83, which correspond to a contraction of ε_r (22 °C) = 15% and to an expansion of ε_z (22 °C) = 21%. Shapes of both contraction and expansion curves in the thermoelastic plot are common for nematic LCEs with an inflexion point at T_{NI} = 57.5 °C related to the clearing temperature of the material, and with no discontinuity when approaching the isotropic state due to the presence of a para-nematic phase induced by the crosslinking process.[30]

Finally, the mechanical actuation was analyzed, by measuring the forces exerted by the micropillar during expansion upon heating and contraction upon cooling (Fig. 7a). The force was measured as a function of time using a dynamometer, while heating the bottom part of the LCE micropillar array. The maximum measured force was F = 20 mN at the set temperature of T_{set} = 90 °C (Fig. 7b). The time needed to reach this maximum force was around t = 2 min, and showed full reversibility and repeatability upon cooling of the LCE micropillar array. The true stress was evaluated as a function of the micropillar temperature, taking into account its cross-section, its dimensional change as a function of temperature, as well as the measured force. The results show a fast growing stress behavior upon reaching the isotropic phase, with a value of σ_t = 5.6 kPa, and a hysteresis factor of 1.1 between the heating and cooling curves (Fig. 7c).

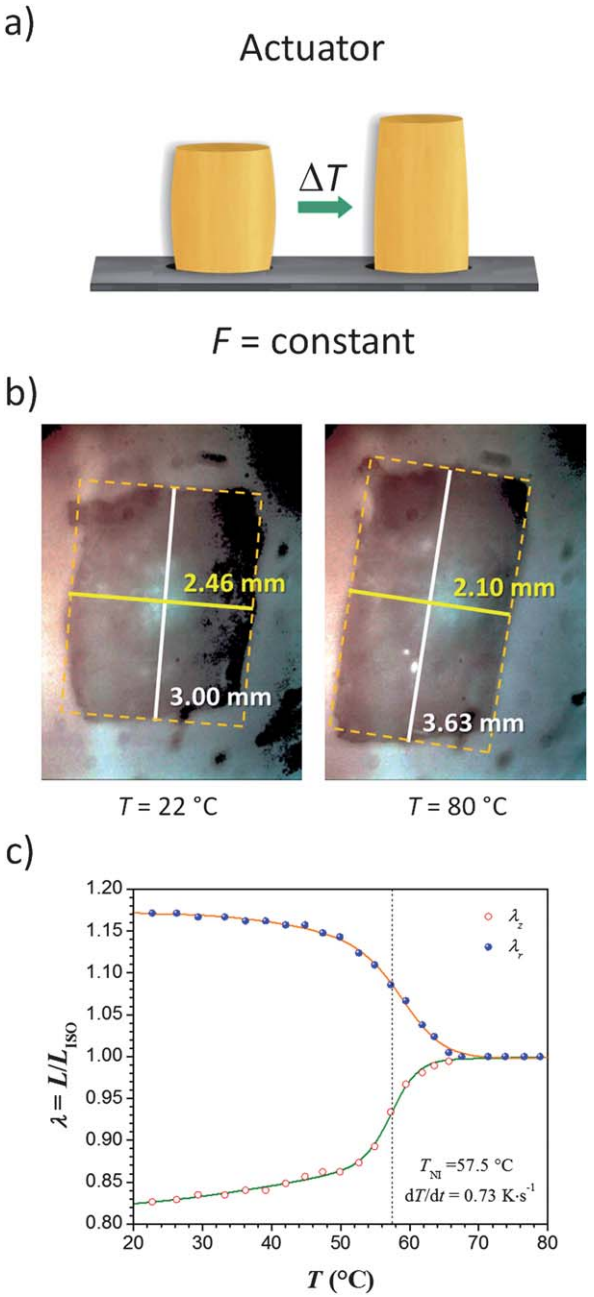

Fig. 6 (a) Actuator principle for the LCE micropillar array. (b) Optical microscopy pictures of one LCE micropillar in the nematic (T = 22 °C) and in the isotropic (T = 80 °C) phases. (c) Thermoelastic experiment on an oriented nematic LCE micropillar showing the expansion along the axial direction of the micropillar (λ_z) and the contraction along the radial direction (λ_r).

All nematic LCE samples reported up to now showed a prolate conformation of the polymer backbone together with a nematic orientation which follows the direction of the applied uniaxial stretching (z-axis) of the sample during the sample preparation. The new nematic LCE sample presented in this work has a two-dimensional prolate polydomain conformation coming from the uniaxial compression (biaxial deformation), which leads to a radial distribution of the polymer backbone and mesogens in the plane (xy-plane). Thus, in the isotropic

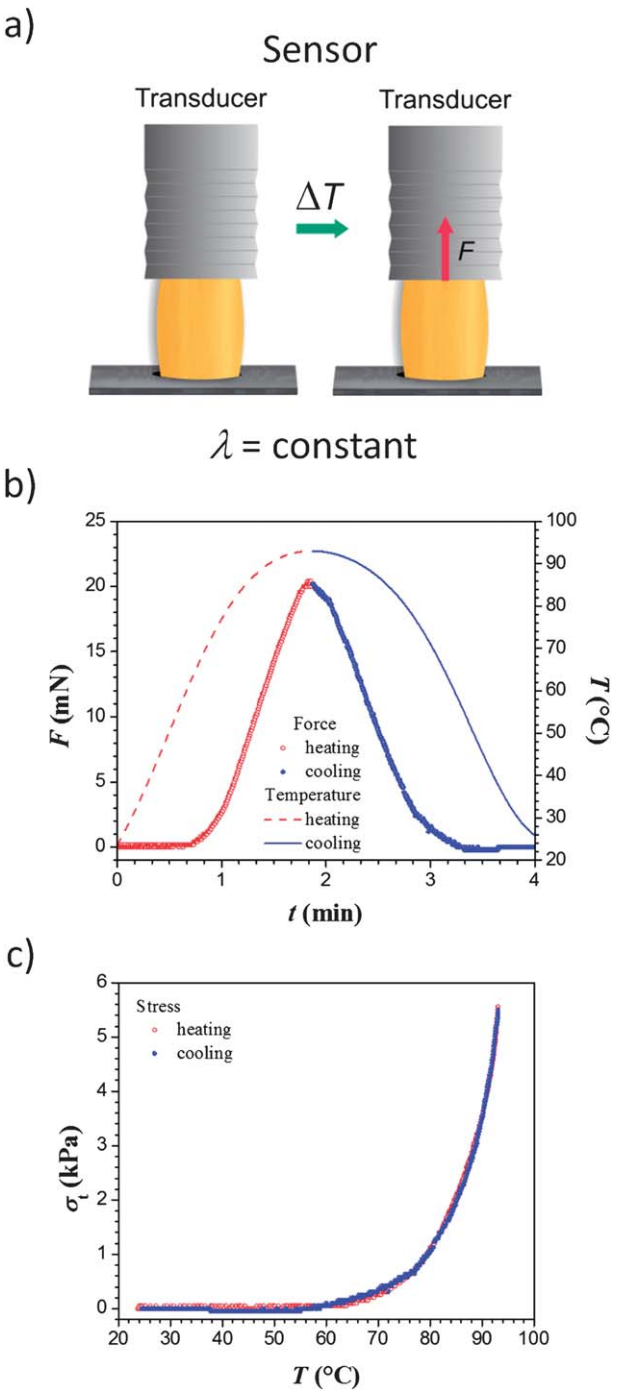

Fig. 7 (a) Sensor principle for the LCE micropillar array. (b) Force as a function of time and (c) stress as a function of temperature during the heating and cooling processes on an oriented nematic LCE micropillar.

state, all previously known nematic LCE samples contract along the *z*-axis, and expand in the other two axes (*x*- and *y*-axis), while being able to lift weight or generate a retractive force upon heating, but not a pushing force upon cooling. Now, for the first time, a nematic LCE sample can expand along the *z*-axis and contract in the other two directions (*x*- and *y*-axes), and the new actuation principle allows LCEs to generate a pushing force and lift a weight upon heating.

The values for the change in height ($\Delta z = 630$ μm), force ($F =$ 20 mN), and stress ($\sigma_t = 5.6$ kPa), together with the processability and tunability of the chemistry in terms of mechanical and thermal actuation, make these LCE optimal materials for haptic applications, and their use as Braille displays.[31] A Braille blister will require micropillars of 1.0–1.2 mm in diameter, a minimum change in height of 300 μm, and minimum forces of 15–30 mN, together with short switching times below the second scale. The energy efficiency and time responsiveness need to be investigated further.

Conclusions

A new LCE micropillar array with two-dimensional prolate polydomain conformation of the polymer backbone and the mesogens has been successfully synthesized. This new concept of the orientation of silicone-based LCE systems by uniaxial compression (biaxial orientation) allows for obtaining micropushers, with actuation temperatures around 55 °C. The two-dimensional prolate polydomain conformation of the LCE micropillars was confirmed by swelling, polarized optical microscopy and X-ray experiments, where the anisotropic swelling value above the unit and the planar distribution of the prolate polymer backbone and nematogens were observed.

The resulting LCE micropillars show an expansion factor of $\varepsilon_z = 21\%$ along the axial direction and a contraction factor of $\varepsilon_r = 15\%$ in the radial direction upon isotropization of the sample. These changes in the dimensions, together with the actuation force of $F = 20$ mN ($\sigma_t = 5.6$ kPa), and the possibility of obtaining different shapes on demand – besides the common LCE strip – make the LCE materials very suitable candidates for haptic applications, as well as for their integration in Microsystem Technology, in the development of complex devices through a batch process.

Acknowledgements

The authors acknowledge partial financial support from the NOMS project, which has been funded by the European Commission under contract number 228916, the financial support from the Generalitat de Catalunya under contract 2009SGR22, and from Universitat Autònoma de Barcelona for predoctoral grant. We also thank Roberta Ceravola for the DSC measurements and Dr Anke Hoffman for allowing us to perform the X-ray experiments, and Jaume Torras for helping us in the cover design.

Notes and references

1 M. Warner and E. M. Terentjev, in *Liquid Crystal Elastomers*, Clarendon, Oxford, 2007, (revised edition).
2 A. Sánchez-Ferrer, A. Merekalov and H. Finkelmann, *Macromol. Rapid Commun.*, 2011, **32**, 672.
3 M. Camacho-López, H. Finkelmann, P. Palffy-Muhoray and M. Shelley, *Nat. Mater.*, 2004, **3**, 307.
4 A. Kaiser, M. Winkler, S. Krause, H. Finkelmann and A. M. Schmidt, *J. Mater. Chem.*, 2009, **19**, 538.

5 J. M. Haberl, A. Sánchez-Ferrer, A. M. Mihut, H. Dietsch, A. M. Hirt and R. Mezzenga, *Adv. Mater.*, 2013, **25**, 1787.
6 M. Chambers, H. Finkelmann, M. Remškar, A. Sánchez-Ferrer, B. Zalar and S. Žumer, *J. Mater. Chem.*, 2009, **19**, 1524.
7 T. Hiscock, M. Warner and P. Palffy-Muhoray, *J. Appl. Phys.*, 2011, **109**, 104506.
8 H. Wermter and H. Finkelmann, *e-Polym.*, 2001, 013.
9 B. Donnio, H. Wermter and H. Finkelmann, *Macromolecules*, 2000, **33**, 7724.
10 P. G. de Gennes, *C. R. Seances Acad. Sci., Ser. B*, 1975, **281**, 101.
11 H. Finkelmann, H. J. Kock and G. Rehage, *Macromol. Rapid Commun.*, 1981, **2**, 317.
12 A. Sánchez-Ferrer and H. Finkelmann, *Mol. Cryst. Liq. Cryst.*, 2009, **508**, 348.
13 A. Sánchez-Ferrer, *Proc. SPIE*, 2011, **8107**, 810702.
14 A. Buguin, M. H. Li, P. Silberzan, B. Ladoux and P. Keller, *J. Am. Chem. Soc.*, 2006, **128**, 1088.
15 C. Ohm, C. Serra and R. Zentel, *Adv. Mater.*, 2009, **21**, 4859.
16 A. Sánchez-Ferrer, T. Fischl, M. Stubenrauch, H. Wurmus, M. Hoffmann and H. Finkelmann, *Macromol. Chem. Phys.*, 2009, **210**, 1671.
17 A. Sánchez-Ferrer, T. Fischl, M. Stubenrauch, A. Albrecht, H. Wurmus, M. Hoffmann and H. Finkelmann, *Adv. Mater.*, 2011, **23**, 4526.
18 C. J. Camargo, H. Campanella, J. E. Marshall, N. Torras, K. Zinoviev, E. M. Terentjev and J. Esteve, *Macromol. Rapid Commun.*, 2011, **32**, 1953.
19 C. J. Camargo, H. Campanella, J. E. Marshall, N. Torras, K. Zinoviev, E. M. Terentjev and J. Esteve, *J. Micromech. Microeng.*, 2012, **22**, 075009.
20 H. Finkelmann, U. Kiechle and G. Rehage, *Mol. Cryst. Liq. Cryst.*, 1983, **94**, 343.
21 J. Küpfer and H. Finkelmann, *Makromol. Chem., Rapid Commun.*, 1991, **12**, 717.
22 J. Küpfer and H. Finkelmann, *Macromol. Chem. Phys.*, 1994, **195**, 1353.
23 H. Finkelmann, A. Greve and M. Warner, *Eur. Phys. J. E: Soft Matter Biol. Phys.*, 2001, **5**, 281.
24 W. Caseri and P. S. Pregosin, *Organometallics*, 1988, **7**, 1373.
25 B. Marciniec, in *Comprehensive Handbook on Hydrosilylation*, Pergamon, Oxford, 1992.
26 R. Lovell and G. R. Mitchell, *Acta Crystallogr., Sect. A: Cryst. Phys., Diffr., Theor. Gen. Crystallogr.*, 1981, **37**, 135.
27 G. R. Mitchell and A. H. Windle, in *Development in Crystalline Polymers-2*, ed. D. C. Basset, Elsevier Applied Science, London, 1988, vol. 3, p. 115.
28 H. Finkelmann, S. T. Kim, A. Muñoz, P. Palffy-Muhoray and B. Taheri, *Adv. Mater.*, 2001, **13**, 1069.
29 S. T. Kim and H. Finkelmann, *Macromol. Rapid Commun.*, 2001, **22**, 429.
30 A. Lebar, Z. Kutnjak, S. Žumer, H. Finkelmann, A. Sánchez-Ferrer and B. Zalar, *Phys. Rev. Lett.*, 2005, **94**, 197801.
31 N. H. Runyan and D. B. Blazie, *Proc. SPIE*, 2011, **8107**, 81070G.